MOLECULAR METABOLISM

LDLR inhibition promotes hepatocellular carcinoma proliferation and metastasis by elevating intracellular cholesterol synthesis through the MEK/ERK signaling pathway

Ziye Chen [1,5,7], Lu Chen [2,5,7], Bo Sun [3,5,7], Dongming Liu [2,5], Yuchao He [1,5], Lisha Qi [4,5], Guangtao Li [1,5], Zhiqiang Han [1,5], Linlin Zhan [1,5], Su Zhang [1,5], Keyun Zhu [1,5], Yi Luo [1,5], Liwei Chen [1,5], Ning Zhang [1,5,6,**], Hua Guo [1,5,*]

ABSTRACT

Objective: Adaptive rewiring of cancer energy metabolism has received increasing attention. By binding with LDLs, LDLRs make most of the circulating cholesterol available for cells to utilize. However, it remains unclear how LDLR works in HCC development by affecting cholesterol metabolism.

Methods: Database analyses and immunohistochemical staining were used to identify the clinical significance of LDLR in HCC. A transcriptome analysis was used to reveal the mechanism of LDLR aberration in HCC progression. A liver orthotopic transplantation model was used to evaluate the role of LDLR in HCC progression in vivo.

Results: Downregulation of LDLR was identified as a negative prognostic factor in human HCC. Reduced expression of LDLR in HCC cell lines impaired LDL uptake but promoted proliferation and metastasis in vitro and in vivo. Mechanistically, increasing intracellular de novo cholesterol biosynthesis was the chief contributor to malignant behaviors caused by LDLR inhibition, which could be rescued by simvastatin. Activation of the MEK/ERK pathway by LDLR downregulation partially contributed to intracellular cholesterol synthesis in HCC.

Conclusions: Downregulation of LDLR may elevate intracellular cholesterol synthesis to accelerate proliferation and motility through a mechanism partially attributed to stimulation of the MEK/ERK signaling pathway. Repression of intracellular cholesterol synthesis with statins may constitute a targetable liability in the context of lower LDLR expression in HCC.

1. INTRODUCTION

Notable progress in cancer research has allowed the characterization of several biological properties of this pathological situation, which were generalized as 10 hallmarks by Robert A. Weinberg in 2011 [1,2]. Specifically, reprogramming energy metabolism has attracted increasing interest as a newly identified cancer feature. The excessive growth and dysplastic characteristics of cancer impose higher demands for energy and substrates [3]. Aerobic glycolysis, as the earliest metabolic alteration detected in cancer, was elucidated by Otto Warburg in the 1920s [4]. Enhanced glucose uptake provides sufficient ATP and intermediates for anabolic reactions benefiting cancer cells [5]. New perspectives on cancer metabolism have been elucidated in the ensuing decades. Continuous nutrient scarcity drives cancer cells

[1]Department of Tumor Cell Biology, Tianjin Medical University Cancer Institute and Hospital, Tianjin, 300060, China [2]Department of Hepatobiliary Cancer, Liver Cancer Research Center, Tianjin Medical University Cancer Institute and Hospital, Tianjin, 300060, China [3]The Second Department of Breast Cancer, Tianjin Medical University Cancer Institute and Hospital, Tianjin, 300060, China [4]Department of Pathology, Tianjin Medical University Cancer Institute and Hospital, Tianjin, 300060, China [5]National Clinical Research Center for Cancer, Key Laboratory of Cancer Prevention and Therapy, Tianjin's Clinical Research Center for Cancer, Tianjin 300060, China [6]Translational Cancer Research Center, Peking University First Hospital, Beijing 100034, China

[7] These authors contributed equally to this study.

*Corresponding author. Tianjin Medical University Cancer Institute and Hospital, Tianjin, 300060, China. Tel.: +86 22 23537796, Fax: +86 22 23537796. E-mail: guohua@tjmuch.com (H. Guo).

**Corresponding author. Tianjin Medical University Cancer Institute and Hospital, Tianjin, 300060, China. Tel.: +86 22 23537796, Fax: +86 22 23537796. E-mail: ningzhangtj@yahoo.com (N. Zhang).

to utilize more kinds of substrates than noncancer cells [6]. Aberrancy of lipid metabolism, for example, has been validated to play an increasingly pivotal role in cancer by providing energy and macromolecules or lipid-mediated signaling [7,8].

As a requisite neutral lipid, cholesterol may help sustain membrane integrity and fluidity or synthesize steroid hormones and bile acids [3]. To meet essential physiological demands, human cells obtain cholesterol both by intracellular de novo synthesis and importing lipoproteins, the main carriers of circulating cholesterol, from the extracellular space [9]. Thus, intracellular cholesterol homeostasis is constantly under rigorous regulation. However, regarding cancer, dysregulation of cholesterol metabolism has been indicated to exist in multiple cancer types, such as breast cancer [10], lymphoma [11], and pancreatic cancer [12].

Hepatic cells typically occupy a vital position in maintaining cholesterol homeostasis within the body. Along with manufacturing the largest amounts of endogenous cholesterol, the liver is also the major site of exogenous lipoprotein endocytosis to maintain serum cholesterol homeostasis [9]. Thus, cholesterol dysregulation is an especially inevitable event in hepatocellular carcinoma (HCC) progression. Dietary cholesterol has been shown to facilitate steatohepatitis-related HCC through dysregulation of metabolism and calcium signaling [13]. Researchers found that among early stage HCCs, the subtype with disrupted cholesterol homeostasis exhibited the worst overall survival and the poorest prognosis compared with the other two subtypes [14].

Instead of existing freely in the circulation, cholesterol is usually packaged within lipoproteins due to its minimally hydrophilic nature, presenting a water-soluble surface and a lipid-soluble core [15]. The protein/lipid ratio helps identify several types of lipoproteins with different densities. Low-density lipoprotein (LDL), the major cholesterol carrier in blood, makes exogenous cholesterol available to cells primarily by binding to its receptor and sequentially forming vesicles via endocytosis [16].

The low-density lipoprotein receptor (LDLR), which acts as a cell-surface glycoprotein, belongs to the LDLR family [17]. Considering the vital role of the LDL/LDLR routine in regulating blood and intracellular cholesterol homeostasis, several studies have focused on the function of LDLR in cancer progression. Lower LDLR expression has been illustrated to indicate worse clinical outcomes in prostate and cervical cancer [18,19]. However, knowledge on how LDLR acts in HCC development by mediating LDL uptake and affecting the intracellular cholesterol homeostatic state remains scarce.

In this study, we demonstrated that downregulation of LDLR was a negative prognostic factor in human HCC. Functionally, reduced expression of LDLR in MHCC 97H and HLE cells impaired LDL uptake but promoted HCC cell proliferation and metastasis in vitro and in vivo. Next, we discovered that mechanistically, increased intracellular de novo cholesterol biosynthesis was the chief contributor to malignant behaviors caused by LDLR inhibition, which could be rescued by simvastatin (a cholesterol synthesis inhibitor). We also revealed that the MEK/ERK signaling pathway might contribute to enhancing cholesterol synthesis under LDLR downregulation in HCC. In summary, our study illuminated the role of LDLR in HCC progression and revealed the possibility that cholesterol biosynthesis may be a targetable liability in the context of lower LDLR expression in HCC.

2. MATERIALS AND METHODS

2.1. Clinical materials
A total of 178 pairs of cancerous and matched non-cancerous paraffin-embedded liver samples were collected from September 2012 to September 2018 at Tianjin Medical University Cancer Institute and Hospital (Tianjin, China), and all were confirmed pathologically by board-certified pathologists. Patients with adjuvant therapy were excluded. Written informed consent was obtained from the recruited patients following the Helsinki Declaration. The entire study was approved by the Tianjin Medical University Cancer Institute and Hospital Ethics Committee.

2.2. Cell cultures
MHCC 97H cells were kindly provided by the Fudan University Liver Cancer Institute in Shanghai, China (RRID: CVCL_4972). HLE from the Health Science Research Resources Bank (Osaka, Japan, RRID: CVCL_JF92), HEK-293T, and HUVEC from the American Type Culture Collection (ATCC, Manassas, VA, USA, RRID: CVCL_ZM06) were purchased separately. DMEM medium (Corning, NY, USA) was added to 10% (vol/vol) fetal bovine serum (FBS, PAN-Seratech) and 1% (vol./vol.) penicillin-streptomycin solution (HyClone) for MHCC 97H, HLE, and HEK-293T. HUVEC was cultured in F12-K medium (Gibco). All the cells were cultured in a 37 °C incubator with 5% CO2. PD98059 (Sigma—Aldrich, St. Louis, MO, USA) was used as an inhibitor of the MEK/ERK signaling pathway and simvastatin (Selleck, S1792) was used to inhibit cholesterol synthesis.

2.3. Stable transfected cell line establishment
293T cells were co-transfected with packaging VSVG and δR plasmids plus expression plasmids (MOCK or sh-LDLR, GeneChem, Shanghai) using PEI (Polysciences, cat. 23966-2) to produce lentivirus. After 48 h of transfection with polybrene (Solarbio), puromycin (Gibco) screening was conducted with a concentration of 2.5 μg/mL (MHCC 97H) or

Table 1 — Univariate and multivariate analyses of prognostic factors associated with OS and DFS in 178 patients with HCC.

HCC patients (n = 178)	Number	Univariate analysis		Multivariate analysis		Univariate analysis		Multivariate analysis	
		5-year OS (%)	P value	HR (95% CI)	P value	5-year DFS (%)	P value	HR (95% CI)	P value
Age (years) > 55/ ≤ 55	89/89	33.7/28.1	0.745			25.8/23.6	0.958		
Sex male/female	148/30	32.4/23.3	0.360			26.4/16.7	0.251		
Liver cirrhosis Y/N	98/80	34.7/26.3	0.225			24.5/25.0	0.919		
Tumor size (cm) > 5/ ≤ 5	70/108	25.7/34.3	**0.037***	1.310 (0.908, 1.891)	0.148	22.9/25.9	0.062		
Mavi Y/N	18/160	11.1/33.1	**0.000***	2.000 (0.799, 5.006)	0.139	5.6/26.9	**0.000***	2.507 (1.082, 5.811)	**0.032***
Mivi Y/N	102/76	24.5/39.5	**0.014***	1.417 (0.978, 2.055)	0.066	22.5/27.6	0.177		
Satellite nodule Y/N	81/97	23.5/39.7	**0.007***	1.306 (0.893, 1.910)	0.168	20.5/27.9	0.171		
BCLC stage 0&A/B&C	152/26	33.6/15.4	**0.001***	1.086 (0.481, 2.455)	0.843	27.6/7.7	**0.000***	1.211 (0.584, 2.512)	0.606
Staining score of LDLR > 1/ ≤ 1	45/133	40.0/27.8	**0.021***	0.644 (0.417, 0.995)	**0.047***	31.1/22.6	**0.037***	0.664 (0.442, 0.996)	**0.048***

Notes: *P value < 0.05 was considered significant.
Abbreviations: HCC, hepatocellular carcinoma; HBV, hepatitis B virus; Mavi, macrovascular invasion; Mivi, microvascular invasion; BCLC, Barcelona Clinic Liver Cancer.

Table 2 — Relationship between clinicopathological characteristics and LDLR expression in 178 patients with HCC.

Characteristics		Total	LDLR expression		P value	Characteristics		Total	LDLR expression		P value
		178	Low	High				178	Low	High	
Age (years)					0.391	**Tumor size (cm)**					0.344
	>55	89	69	20			>5	70	55	15	
	≤55	89	64	25			≤ 5	108	78	30	
Sex					0.517	**Mavi**					**0.049***
	Male	148	112	36			Present	18	16	2	
	Female	30	21	9			Absent	160	117	43	
Liver cirrhosis					0.938	**BCLC stage**					**0.026***
	Present	98	73	25			0&A	152	109	43	
	Absent	80	60	20			B&C	26	24	2	
Satellite nodule					**0.025***						
	Present	81	67	14							
	Absent	97	66	31							

Notes: *P value < 0.05 was considered significant.
Abbreviations: HCC, hepatocellular carcinoma; HBV, hepatitis B virus; Mavi, macrovascular invasion; Mivi, microvascular invasion; BCLC, Barcelona Clinic Liver Cancer.

1 μg/mL (HLE) for 7 days. Efficiency validation was performed by Western blotting.

2.4. Western blotting

Cells were rinsed three times with pre-cold PBS at an 80% fusion rate followed by a 30-min lysis on ice with SDS lysis buffer replenished with protease inhibitor cocktail (Roche,11873580001). Protein samples were loaded into wells in SDS-PAGE gel to separate into bands under a voltage of 60 V—120 V. Electroblotting helped pull the proteins onto a polyvinylidene difluoride membrane (Immobilon-P, Millipore, Billerica, MA, USA), which was accessible to antibody. Then 5% non-fat milk was involved in blocking non-specific binding. Chemiluminescent detection with ECL (Pierce, Rockford, IL, USA) was performed after incubation with specific primary antibodies at 4 °C overnight and secondary antibodies at room temperature for 1 h.
The antibodies involved are listed as follows: LDLR (ab52818, 1:1000, RRID: AB_881213), GAPDH (sc-47724, 1:1000, RRID: AB_627678), MEK-1/2 (sc-81504,1:500, RRID: AB_1126111), p-MEK-1/2 (Ser 218/Ser 222) (sc-7995, 1:1000, RRID: AB_2234805), Erk 1/2 (9102S, 1:1000, RRID: AB_330744), p-Erk 1/2 (Thr 202/Tyr204) (4370S, 1:1000, RRID: AB_2315112), cyclin B1 (4138T, 1:1000, RRID:AB_2072132), cyclin D1 (55506S, 1:1000, RRID:AB_2827374), HRP-conjugated anti-mouse (sc-2005,1:4000, RRID: AB_631736), HRP-conjugated anti-rabbit (sc-2004, 1:4000, RRID: AB_631746), and HRP-conjugated anti-goat (sc-2020, 1:4000, RRID: AB_631728). All the measurements were detected in triplicate.

2.5. Proliferation and colony-formation assays

A total of 2×10^3 cells/well were seeded in 96-well plates before incubating with Cell Counting Kit-8 (CCK-8, 10 μl/well, Dojindo Laboratories, Japan) at different time points. Another 4 to 5 parallel wells were set for difference exclusion. The optical density at 450 nm was read using an enzyme labeler (BioTek Synergy H1, Burlington, VT, USA).
Next, 300 cells/well were planted into a 12-well plate and cultured for 2—3 weeks to calculate the clone number. Then 2—3 weeks later, the colony was rinsed 3 times with PBS, fixed with 4% paraformaldehyde (PFA, Solarbio), and stained with 0.5% crystal violet (Solarbio). Pictures were obtained with a digital camera. All of the measurements were detected in triplicate.

2.6. Cell cycle detection

Cells treated with or without simvastatin were digested and washed once with PBS. Then cell suspensions in 50 μl of PBS were added to 95% ethanol and maintained at 4 °C overnight. The next day, the cells were stained with 500 μL of propidium iodide (PI, BD Biosciences, RRID: AB_2869075) after centrifugation and incubated in the dark for more than 30 min. The samples were analyzed on a flow cytometer (BD). The data were analyzed using ModFit LT 4.0.

2.7. Migration assay

A total of 1.5×10^6 cells/well were plated into a 6-well plate to measure their migration ability. After they attached onto the plate, the cells were straight scratched with a 10-μl pipette tip. Floating cells were ejected with PBS and supplemented with DMEM with 2% FBS. Distances were measured at different time points for 24 h—48 h and recorded by a light microscope. All the measurements were detected in triplicate.

2.8. Motility monitoring by a high-content screening system (HCS)

For the high-content screening system (HCS, PerkinElmer), 5000 cells/well with two replicates were plated into a six-well plate. Once the cell shape was scratched the next day, dynamic imaging of viable cells was performed in the HCS for 18 h. Displacement parameters or average migration distances were analyzed automatically using Harmony software. All the measurements were detected in triplicate.

2.9. Chemotaxis and invasion assays

Cell suspensions containing 5×10^5 cells in DMEM containing 2% FBS were plated into the upper space of an 8-μm chamber (Falcon Cell Culture Inserts, Corning) with or without diluted Matrigel. The lower chamber holding a 24-well plate was filled with DMEM containing 20% FBS. After incubation for approximately 40 h in a 37 °C incubator, the contents were cleaned with PBS and the chamber membrane was fixed and rinsed before being stained. Random fields were captured by an optical microscope for cell quantification. All the measurements were detected in triplicate.

2.10. RNA extraction and quantitative RT-PCR (qPCR)

TRIzol reagent (Ambion, Austin, TX, USA) was used to extract the total RNA from adherent cells or frozen clinical samples according to the manufacturer's guidelines. RNA quantification was achieved using a

Table 3 — Primers for target genes involved in the quantitative RT-PCR.

Primer	Sequence (5′ to 3′)	Primer	Sequence (5′ to 3′)
LDLR-Forward	GCCTCTGAAATGCCTCTTCT	SOAT1-Forward	GCAGGCTTACCTATTTCTACTC
LDLR-Reverse	CCCAGAAGCCACTCATACATAC	SOAT1-Reverse	CAGTTAGCCCGTCTTTTACAATC
HMGCR-Forward	TACCATGTCAGGGGTACGTC	ABCA1-Forward	ACATCCTGAAGCCAATCCTGA
HMGCR-Reverse	CAAGCCTAGAGACATAAT	ABCA1-Reverse	CTCCTGTCGCATGTCACTCC
SQLE-Forward	TCCTTGCTCAGGCTCTTTATG	MYO5B-Forward	AAGGAGACAAGAGCCTACAGC
SQLE-Reverse	AGGGTTAGGAGACAATACAGAAAG	MYO5B-Reverse	TGGATTCCGTAAGAAGGGCAG
DHCR24-Forward	ATGCACTCCGTCCGAAAACT	LIMA1-Forward	GACTCCCAGGTTAAGAGTGAGG
DHCR24-Reverse	TCGAAACGCAGCTTGACGTA	LIMA1-Reverse	TTGCAGGTGCCTGAAACTTCT
HMGCS1-Forward	GATGTGGGAATTGTTGCCCTT	APOB-Forward	TGCTCCACTCACTTTACCGTC
HMGCS1-Reverse	ATTGTCTCTGTTCCAACTTCCAG	APOB-Reverse	TAGCGTCCAGTGTGTACTGAC
NSDHL-Forward	AGGCAGCCAGGAACGGCAAGAT	APOC1-Forward	TGGAGAGCATACCGGATAAACT
NSDHL-Reverse	GAAATGCCTTCCCACCCAGTGTCGA	APOC1-Reverse	AGGAGAACGTGGTCTTCAACT
CYP26B1-Forward	GGCAACGTGTTCAAGACGC	GAPDH-Forward	TGGTATCGTGGAAGGACTCA
CYP26B1-Reverse	TGCTCGCCCATGAGGATCT	GAPDH-Reverse	CCAGTAGAGGCAGGGATGAT
SREBF2-Forward	CCCTTCAGTGCAACGGTCATTCAC		
SREBF2-Reverse	TGCCATTGGCCGTTTGTGTC		

NanoDrop spectrophotometer (NanoDrop Technologies, Wilmington, DE, USA). cDNA was synthesized with PrimeScript RT Master Mix (TaKaRa, Japan). Quantitative RT-PCR (qPCR) using AceQ SYBR qPCR Master Mix (Vazyme, Q111) was carried out as instructed with a Bio-Rad CFX96 system. The primers involved are listed in Table 3.

2.11. Dil-LDL uptake
Cells with differential LDLR expression were seeded into a 6-well plate and cultured in a 37 °C incubator overnight before tracking their LDL uptake ability. After a 24-h starvation, diluted Dil-LDL (5 μg/mL, Molecular Probes) was added to the plate for 2 h. Excess DiI probes were washed away and cells were fixed with 4% PFA. Cell nuclei were indicated with DAPI (Solarbio) and prolonged gold anti-fade reagent (Invitrogen). Random fields were captured by a fluorescence microscope. The experiments were detected in triplicate.

2.12. Filipin staining
A total of 5×10^4 cells/well were seeded onto a sterile slide (Solarbio) placed in a 12-well plate and incubated at 37 °C overnight. After being fixed by 4% PFA, the cells were stained for 2 h with filipin (50 μg/mL, Sigma). Forty microliters/slide of prolonged gold anti-fade reagent (Invitrogen) was used to mount the cells. A DAPI filter was required to view the filipin staining. A fluorescence microscope (Zeiss) was used to scan and record the fluorescence. The experiments were detected in triplicate.

2.13. PD98059 treatment
A total of $6-7 \times 10^5$ cells/well were seeded in 6-well plates. After they attached to the plate, the cells were starved with DMEM basic medium for 12 h. Then the cells were incubated with basic medium with 0.5% FBS added to 25 μM of PD98059 in a 37 °C incubator for 48 h before protein extraction or conditional medium acquisition.

2.14. Conditional medium acquisition
MHCC 97H with different LDLR levels was cultured in a 10-cm dish at 80% confluence overnight and then complete medium was changed into fresh serum-free media for 24 h. The supernatant was collected and centrifuged at 1300 g to eliminate debris. Aliquots were stored at −20 °C after sterilization with 0.22-μm filters (Millipore, Billerica, MA, USA) until use. Purified CM was mixed with the original medium at different ratios before use.

2.15. Tubule formation
After culturing in conditional medium for 24 h, HUVECs were seeded into a 48-well plate coated with Matrigel at a density of $2-3 \times 10^4$/ well. Tube formation was observed at different time points with a light microscope (Leica). The experiments were independently performed in triplicate.

2.16. Immunohistochemistry (IHC) and multiplex IHC
Paraffin-embedded HCC slices were acquired from the Tianjin Medical University Cancer Institute and Hospital. Deparaffinization was achieved with xylene and ethanol in decreasing concentrations. Antigen retrieval with citrate buffer was required to expose epitopes to antibody. Then 3% H_2O_2 was used to block endogenous peroxidase before antibody specific to LDLR (ab52818, RRID: AB_881213), Ki67 (ab16667, RRID: AB_302459), and HMGCR (Proteintech 13533-1-AP, RRID: AB_2877957) slices overnight in 4 °C. (Other antibodies involved are listed in Section 2.4). Signals of the target antigen were amplified with a secondary antibody PV-6001 kit (Zhongshan Biotechnology, Beijing, China) in a 37 °C incubator for 1 h and developed in a DAB detection kit (Zhongshan Biotechnology, Beijing, China) with hematoxylin counterstaining to indicate the nuclei.

The LDLR expression level was assessed using the staining intensity (zero for negative, one for weak, two for medium, and three for strong). Pictures were captured by a fluorescence microscope (Olympus BX61, Tokyo, Japan) at different objectives.

2.17. Animals

2.17.1. Animal rights
All the animal experiments were conducted in accordance with the National Institutes of Health Guidelines for the Care and use of Laboratory Animals (NIH Publication No. 8023, revised 1978) and performed in accordance with guidelines approved by the Ethics Committee of Tianjin Medical University Cancer Institute and Hospital. Mice were maintained in a purpose-built facility on a 12-h light/dark cycle with continual access to food and water.

2.17.2. Liver orthotopic transplantation model
Four-week-old male nude mice were purchased from SPF Biotechnology (Beijing, China). MHCC 97H with different LDLR levels was prepared for subcutaneous injection of 5×10^6/mouse to develop implanted tumors. An orthotopic transplantation model was performed

following a previous report [20]. Six-week-old male nude mice (SPF Biotechnology) were randomly divided into 3 groups that contained 10 mice per group. Subcutaneous injection-derived tumors were cut into small pieces ($2 \times 2 \times 2$ mm^3) in cold saline solution. Sequentially, absorbable sutures anchored the tissue pieces to the livers of the mice under anesthesia, with 10 mice for the MOCK group and 20 mice for the LDLR_KD groups. Two weeks later, simvastatin (Selleck) was administered to one of the LDLR_KD groups (50 mg/kg every 2 days). Control solvent treatment was performed in the MOCK and other LDLR_KD groups. Four weeks later, the livers of all of the mice with tumors were resected. Tissues were fixed in 4% PFA for paraffin sections.

2.17.3. Lung metastasis evaluation

Six-week-old male nude mice were purchased from SPF Biotechnology (Beijing, China) with 6 mice for each group. MHCC 97H with different LDLR levels was prepared for tail vein injection. One month later, the lungs of all mice were resected. Tissues were fixed in 4% PFA for hematoxylin-eosin staining (H&E).

2.18. RNA-seq and bioinformatic analysis

Total RNA was extracted from MHCC 97H with different LDLR expressions (MOCK vs LDLR_KD) using TRIzol reagent (Ambion) with three biological replicates for each group. RNA purity and integrity were assessed with a NanoPhotometer spectrophotometer (Implen, Westlake Village, CA, USA) and an RNA Nano 6000 Assay kit in a Bioanalyzer 2100 system (Agilent Technologies, Santa Clara, CA, USA), respectively. According to the manufacturer's instructions, sequencing libraries were generated using a NEBNext Ultra RNA Library Prep kit for Illumina (NEB, Ipswich, MA, USA). Briefly, mRNA from the total RNA was purified with poly-T oligo-attached magnetic beads. Library fragments and PCR products were purified with an AMPure XP system (Beckman Coulter, Beverly, MA, USA). Library quality was assessed on a Agilent Bioanalyzer 2100 system and library preparations were sequenced on an Illumina HiSeq platform.

Downstream analyses were based on high-quality clean reads. Hisat2 was selected as the mapping tool. Differential expression analysis was performed using the edgeR R package (3.18.1). To control the false discovery rate, Benjamini and Hochberg's approach was used to adjust the P values. A corrected P value of 0.05 and an absolute foldchange of two were considered the threshold for significantly differential expression. Other enrichment analysis was implemented using the clusterProfiler R package.

2.19. Database analysis

The TCGA database (RRID:SCR_003193) and dataset in Oncomine (RRID: SCR_007834) were used to analyze the expression profiles of LDLR in HCC. An overall survival analysis of LDLR in HCC was achieved with the Kaplan−Meier plotter (http://www.kmplot.com, RRID: SCR_018753).

A gene set enrichment analysis (GSEA) was run on GSEA 4.0.0 (Broad Institute of MIT and Harvard, RRID: SCR_003199) to analyze the metastasis status (GEO: GSE2564) with different LDLR levels in HCC.

2.20. Statistical analysis

Data were presented as mean $\pm$ SD and statistical significance was defined as $P < 0.05$. Differential comparisons among the groups were fulfilled with two-tailed Student's t test or one-way ANOVA. Correlation was calculated using Spearman's correlation coefficient. For clinical sample data, the overall survival (OS) and disease-free survival (DFS) states were assessed by the Kaplan−Meier method. The period was counted from the surgery date to death (OS), recurrence (DFS), or end of follow-up. An adjusted multivariate Cox regression was designed to analyze the prognostic factors. SPSS 25.0 (SPSS Inc., Chicago, IL, USA) and GraphPad Prism version 8 software were mainly involved.

3. RESULTS

3.1. Downregulation of LDLR was identified as a negative prognostic factor in human HCC

To investigate how LDLR is involved in HCC progression, the expression profile of LDLR in HCC was assessed in published databases and clinical tissues. The Cancer Genome Atlas (TCGA) database analysis revealed a lower expression of LDLR in HCC tissues than in paired noncancerous regions (Figure 1A). We further revealed a tissue-specific expression profile of LDLR. Analysis of a dataset (the Chen liver cohort) from the Oncomine database revealed a decreasing trend in LDLR expression from the normal liver tissue to the primary liver cancer site to sites of distant liver metastasis (Figure 1B) in the samples grouped by cancer sites. According to survival data acquired from the Kaplan−Meier database (http://www.kmplot.com), lower LDLR expression was associated with poor overall survival in HCC patients ($P = 0.014$, Figure 1C). The metastasis data in the GEO dataset (GSE2564) also confirmed the negative prognostic role of lower LDLR (Figure 1D). Closer evaluation of the clinical samples by qPCR and histological analysis further solidified these findings. Twenty-seven pairs of fresh frozen HCC tissues were assessed for the LDLR expression patterns. A lower expression of LDLR was consistently found in most of the tumor tissues compared to the matched paratumor tissues (21/27, Figure 1E). Regarding histological analysis, a unique relationship between the expression of LDLR and the prognosis of HCC patients was further validated in the IHC staining cohort. When evaluated separately, 133 of the 178 patients showed negative ($n = 64$, 36.0%) or weak ($n = 69$, 38.8%) LDLR staining, while 45 patients exhibited moderate ($n = 42$, 23.6%) or strong ($n = 3$, 1.6%) staining (Figure 1F and Figs. S1A−B). Representative photomicrographs of tissues with different LDLR expression levels are shown in Figure 1G.

Associations of the LDLR expression with various clinicopathological factors were then assessed. We first identified that the LDLR staining status varied with the BCLC stage. In total, among 26 patients staged as BCLC B&C, 24 (92.3%) had lower LDLR expression; however, among HCC patients staged as BCLC 0&A, the percentage of patients with lower LDLR was 71.7% (109/152) ($P = 0.026$, Figure 1H, and Table S2). We next separately analyzed the correlation of the LDLR expression with the metastatic ability by assessing the satellite nodule status and with proliferation ability by Ki67 staining. Sixty-seven of the 81 (82.7%) patients with positive satellite nodules showed lower LDLR expression. In contrast, only 68.0% (66/97) of patients with negative satellite nodules exhibited lower LDLR expression ($P = 0.025$, Figure 1H, and Table 2). A negative correlation was defined between the LDLR expression and Ki67 intensity (Spearman's $r = -0.211$, $P = 0.025$, and Figure 1I−J). Serum AST and ALT levels were much higher in the lower LDLR expression group, indicating functional liver impairment ($P = 0.007/P = 0.002$, Fig. S1C). The Cox regression model showed that a lower expression of LDLR was an independent risk factor for both OS and DFS in HCC (Table 1). Patients with lower levels of LDLR achieved shorter OS (27.8% vs 40.0%, $P = 0.021$) and DFS times (22.6% vs 31.1%, $P = 0.037$) than those in the higher expression cohort (Figure 1K and Table 1). Survival analyses of patients stratified by subtype revealed a specific prognostic role of LDLR in HCC. As shown, lower LDLR expression particularly predicted poor
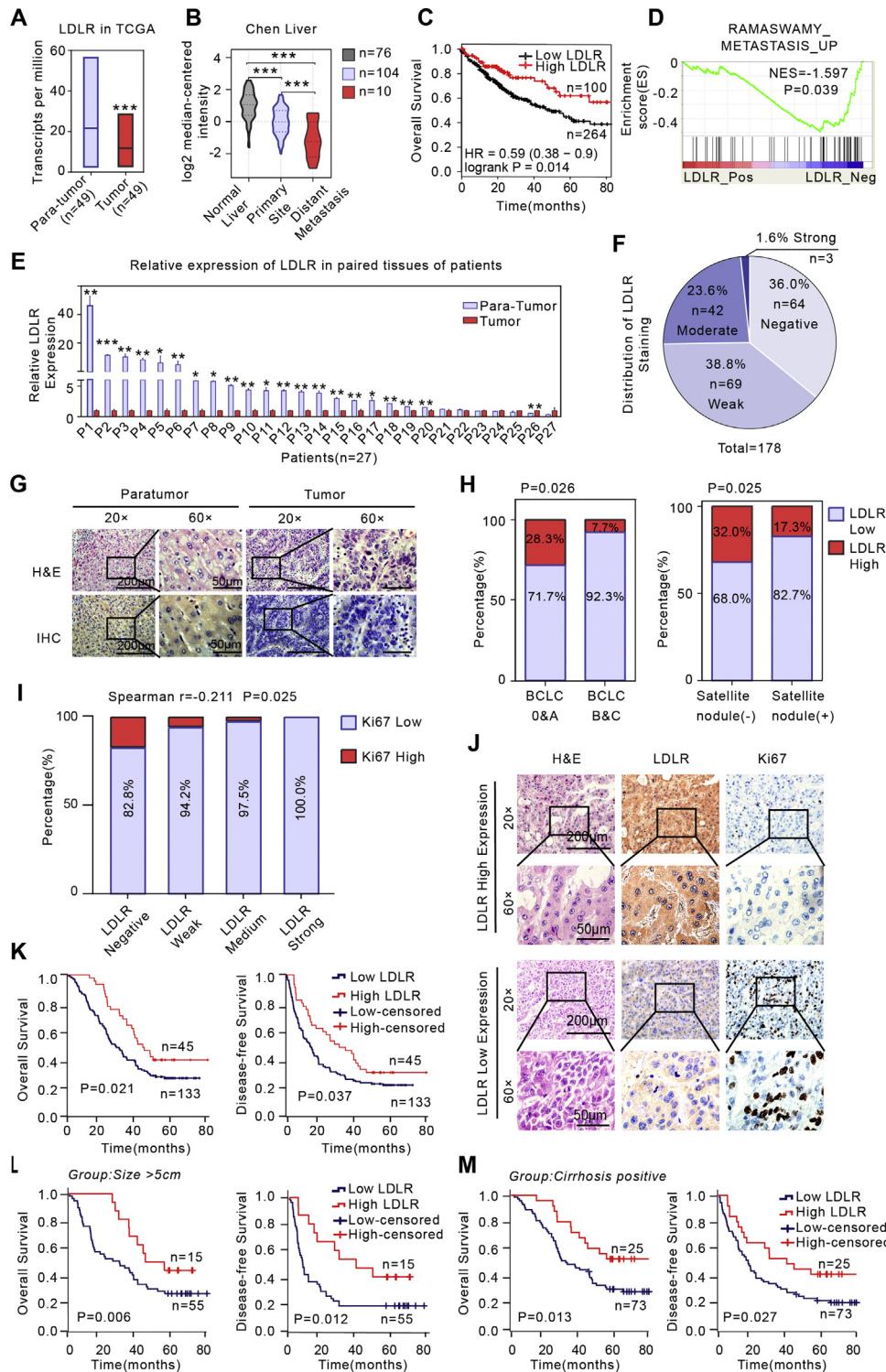
Figure 1: Downregulation of LDLR was identified as a negative prognostic factor in human HCC. (A) TCGA analysis of LDLR expression in HCC cancerous tissues vs paired adjacent regions. (B) LDLR expression pattern validation among normal liver, primary HCC cancer site, and distant metastasis by the Chen liver cohort from Oncomine. (C) Kaplan—Meier analysis of OS based on LDLR levels of HCC patients in the Kaplan—Meier plotter. (D) GSEA of the correlation between LDLR expression and tumor metastasis in the Ramaswamy cohort. (E) qPCR showing differential expression of LDLR in 27 pairs of freshly frozen HCC and matched adjacent tissues. (F) Pie chart showing the distribution of LDLR IHC staining intensity. (G) Representative pictures of H&E and IHC staining for LDLR in cancerous and paired adjacent tissues. Scale bars, 200 μm and 50 μm. (H) Proportions of patients with different LDLR levels according to the BCLC stage or satellite status. (I) Proportions of patients with different Ki67 staining intensity grouped by LDLR staining scores. (J) Representative pictures of H&E and IHC staining for LDLR and Ki67 in matched cancerous tissues. Scale bars, 200 μm and 50 μm. (K) Kaplan—Meier analysis of OS and DFS based on different LDLR levels in 178 HCC clinical samples. (L—M) Kaplan—Meier analysis of OS and DFS based on different LDLR levels in subgroups with tumor sizes exceeding 5 cm (L) or positive cirrhosis status (M). Data are presented as mean ± SD. *P < 0.05, **P < 0.01, and ***P < 0.001. LDLR, low-density lipoprotein receptor; H&E, hematoxylin and eosin; IHC, immunohistochemistry; OS, overall survival; DFS, disease free survival; GSEA, gene set enrichment analysis.

OS and DFS in subgroups with a tumor size exceeding 5 cm (P = 0.006/P = 0.012, Figure 1L, and Fig. S1D) or positive cirrhosis (P = 0.013/P = 0.027, Figure 1M, and Fig. S1E).

This series of results indicated that downregulation of LDLR was a negative prognostic factor with special biological significance in HCC patients.

3.2. Reduced expression of LDLR led to LDL uptake impairment of HCC cells in vitro

To further investigate the role of LDLR in HCC tumor progression, we selected two wild-type HCC cell lines (MHCC 97H and HLE) to generate cell lines with stable LDLR downregulation (LDLR_KD) and matched control cell lines (MOCK) via lentivirus transfection. Deletion efficiencies were confirmed by Western blotting analysis (Figure 2A).

Considering the specific biological functions of LDLR, we collected culture medium from cells with different LDLR levels to evaluate whether the LDL level changed. We consistently found that the LDL content in the medium was significantly elevated in the LDLR_KD groups in the MHCC 97H and HLE cells (Figure 2B and Fig. S1F), which indicated that our intervention altering the LDLR expression was functionally successful. To further verify this result, we incubated the transfected cells with DiI-LDL, fluorescently labeled LDL complexes, which are useful tools for counting cell-surface LDLRs based on the LDL/LDLR binding property. We observed a lower fluorescence intensity in the LDLR_KD groups than in the matched control groups (Figure 2C), which indicated that the cell surface LDLRs were evidently reduced in the LDLR_KD groups in the HLE and MHCC 97H and the LDL uptake ability was efficiently impaired.
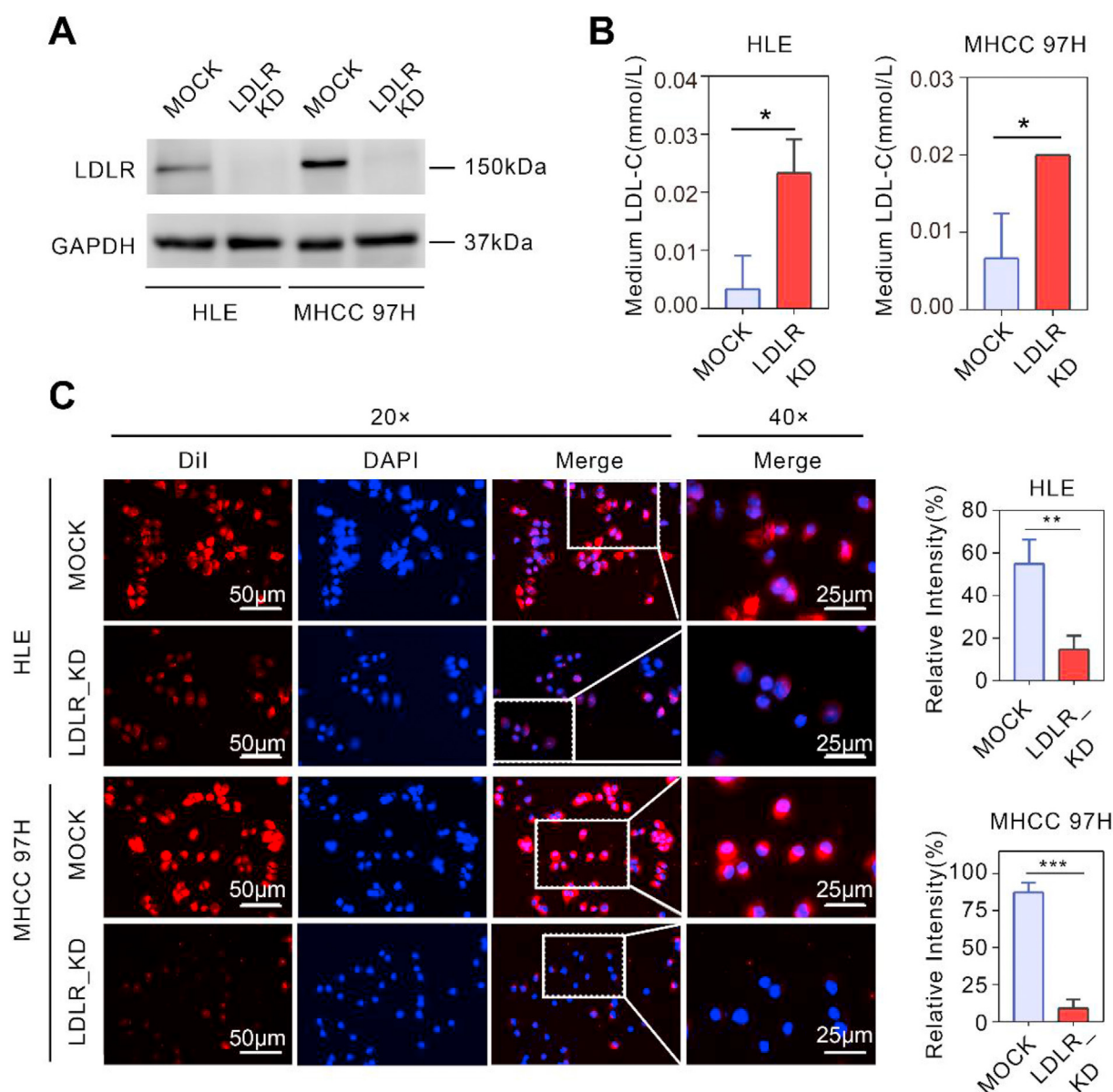
Figure 2: Reduced expression of LDLR led to LDL uptake impairment in vitro. (A) Downregulation efficiency of LDLR in HLE and MHCC97H validated by Western blotting. (B) Test of LDL-C in medium cultured HLE and MHCC 97H with differential LDLR levels. (C) Representative pictures and statistical analysis of DiI fluorescent intensity by DiI-LDL incubation (5 μg/mL) with HLE or MHCC 97H for 2 h at 37 °C. Scale bars, 50 μm and 25 μm. Data are presented as mean ± SD. *P < 0.05, **P < 0.01, and ***P < 0.001. DiI-LDL, 1,1′-diocta-decyl-3,3,3′,3′-tetramethyl-indocarbocyanine perchlorate-labeled LDL. All the measurements were detected in triplicate.
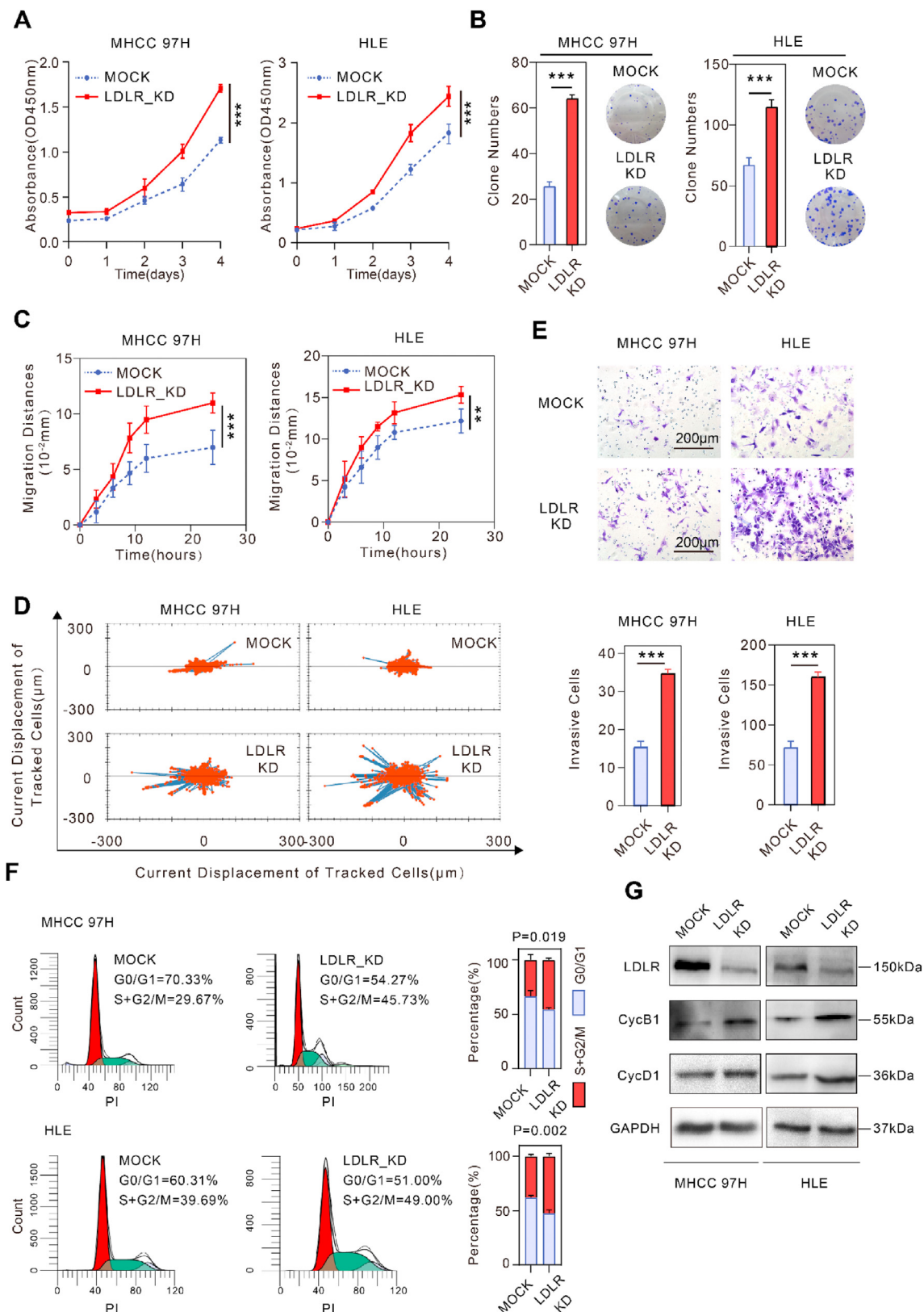
Figure 3: Reduced expression of LDLR promoted proliferation and metastasis of MHCC 97H and HLE in vitro. (A) Cell viability of MHCC 97H and HLE with differential LDLR levels detected by CCK-8 assays at different time points for 96 h. (B) Representative pictures and quantification results of colony-formation assays in MHCC 97H and HLE with differential LDLR levels. (C) Quantification of wound-healing assays in MHCC 97H and HLE with differential LDLR levels. (D) Displacements of viable cells monitored by dynamic imaging with HCS for 18 h. (E) Representative pictures and quantification results of invasion assays in MHCC 97H and HLE with differential LDLR levels. Scale bars, 200 μm. (F) The cell cycle distribution of MHCC 97H and HLE with different LDLR levels. (G) Western blotting of cell cycle-related proteins in MHCC 97H and HLE with different LDLR levels. Data are presented as mean ± SD. *P < 0.05, **P < 0.01, and ***P < 0.001; ns, not significant. HCS, high-content screening system. All of the measurements were detected in triplicate.
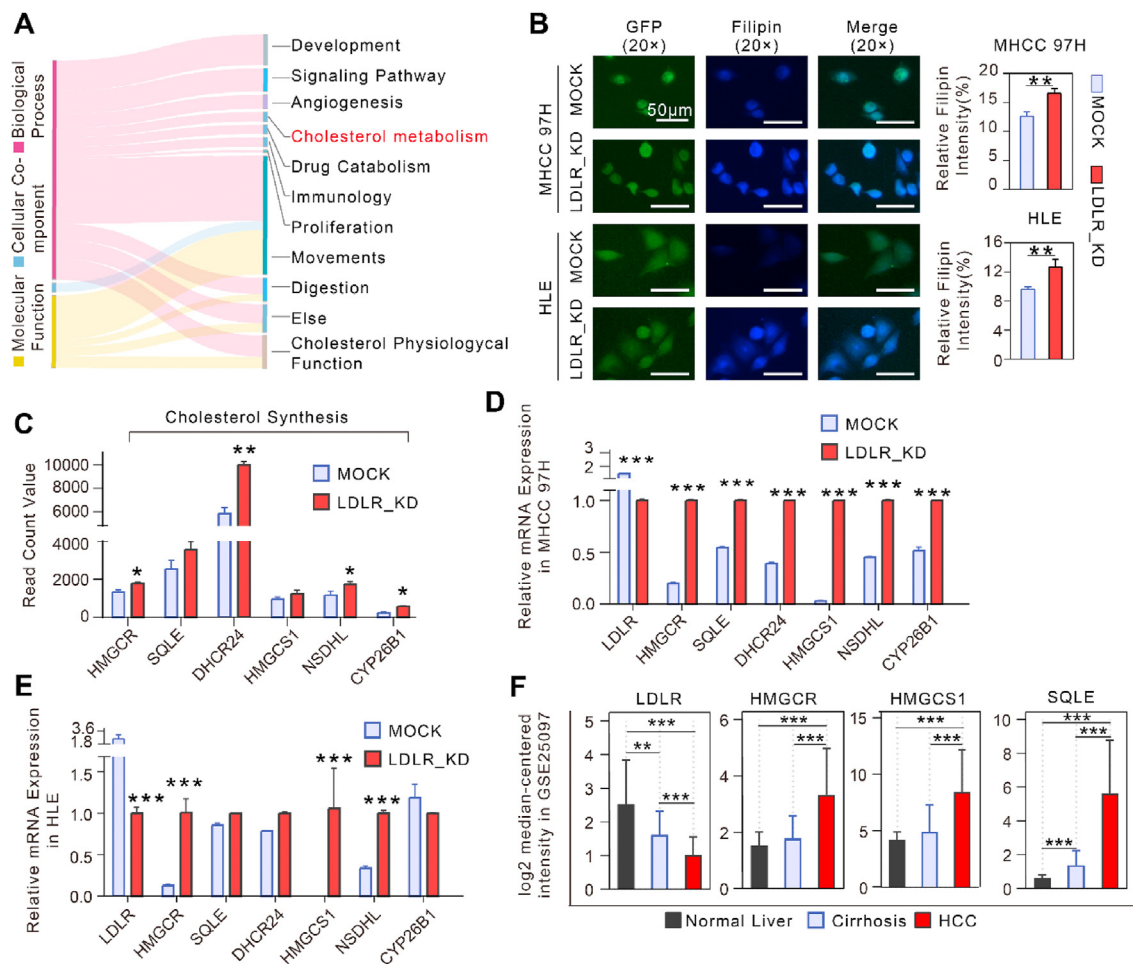
Figure 4: Increased cholesterol biosynthesis was the chief contributor to the malignant behaviors caused by LDLR reduction. (A) Sankey diagram presenting the classification of significantly upregulated pathways defined by GO enrichment analysis. Molecular function is presented in yellow, cellular component in blue, and biological processes in pink. (B) Fluorescence micrographs and quantification of filipin showing the variance of intracellular cholesterol level upon differential LDLR levels in MHCC 97H and HLE. Scale bars, 200 μm. (C) Read count values of differential genes involving cholesterol synthesis screened by transcriptome sequencing. (D—E) RT-PCR showing relative mRNA expression of genes in MHCC 97H (D) and HLE (E) with differential LDLR expression. (F) Expression patterns of the genes involving cholesterol synthesis among normal liver, cirrhotic liver, and HCC in GSE25097. Data are presented as mean ± SD. *P < 0.05, **P < 0.01, and ***P < 0.001; ns, not significant.

In conclusion, a reduced expression of LDLR in HCC cells impaired the transport of extracellular LDL into cells.

3.3. LDLR inhibition facilitated the proliferation and metastasis abilities of HCC cells in vitro

We then further investigated the biological functions of LDLR in the MHCC 97H and HLE cells. Reduced LDLR expression significantly accelerated proliferation in the LDLR_KD groups compared with the MOCK group based on the CCK-8 and colony-formation assay results in the MHCC 97H and HLE cells (Figure 3A—B). The wound-healing assay confirmed that lower LDLR expression enhanced the non-directional migration ability of the MHCC 97H and HLE cells (Figure 3C). In addition, using the high-content cell imaging and analysis system (high-content screening, HCS) allowed the single-cell detection of target cells through an automated cell imaging analysis on the premise of maintaining cellular structural and functional integrity. The label-free analysis module of the HCS system makes long-term dynamic imaging observations possible, and Harmony software helps automatically track the migration of cancer cells. Therefore, we performed dynamic imaging of viable cells with different LDLR levels using the HCS system and obtained the single-cell mobility parameters in each group. In accordance with the data shown in Figure 3C, the higher mobility of the LDLR_KD groups was confirmed in the MHCC 97H and HLE cells as expected (Figure 3D). The invasion assay verified that down-regulation of LDLR expression enhanced the migration and invasion abilities of the MHCC 97H and HLE cells, respectively (Figure 3E). Flow cytometric analysis of cell cycles revealed the cell cycle distribution change in the LDLR-KD cells. We observed that the LDLR_KD cells entered the cell cycle with a decreased percentage of G0/G1-phase cells accompanied by S + G2/M phase extension in the MHCC 97H and HLE (Figure 3F). We also tested the cell cycle-related proteins cyclin B1 and cyclin D1 expression by Western blotting in the LDLR-KD cells. Accordingly, the protein levels of cyclin B1 and cyclin D1 were both upregulated under LDLR downregulation (Figure 3G and Fig. S1G). These phenomena indicated that LDLR downregulation promoted the proliferation and metastasis of HCC cells in vitro, in accordance with the negative prognostic role of lower LDLR identified by the previously mentioned online database analyses and clinical sample validation.

3.4. Increased cholesterol synthesis chiefly promoted the malignant behaviors caused by lower LDLR

To mechanistically explain these findings, we carried out transcriptome sequencing using MHCC 97H cell lines with different LDLR levels. The hierarchical cluster analysis results and correlation heat map indicated an obvious intergroup difference and high intragroup similarity (Figs. S2A—B). We also identified pathways concerning the positive regulation of cell proliferation and migration (Figs. S2C—D), which were in accordance with the in vitro functional results (Figure 3A—E). Considering the contradiction between the high cholesterol demand to support malignant behaviors (Figure 3A—F) and impaired LDL uptake caused by LDLR downregulation (Figure 2A—C), we hypothesized that intracellular alteration in cholesterol metabolism might exist to fulfill the requirements for augmented biological activities. As expected, we identified several cholesterol metabolism pathways upregulated in the LDLR_KD groups using the Gene Ontology (GO) enrichment analysis (Figure 4A). We then stained slides of cells with different LDLR levels with filipin, which is highly fluorescent, binds specifically to cholesterol, and has found widespread use as a histochemical stain for intracellular cholesterol [21]. More intracellular cholesterol was visualized in the LDLR_KD groups than in the control groups of the MHCC 97H and HLE cells (Figure 4B), which indicated the increased requirements for cholesterol existed on the background of augmented biological activities caused by LDLR downregulation.

It is well established that intracellular homeostasis regulation mainly consists of biosynthesis, esterification, intake, and excretion [9]. We thus measured the mRNA levels of key genes involved in the aforementioned processes to ascertain the mainly functioning processes. The most significant increases were focused on genes related to cholesterol biosynthetic processes, including *HMGCR*, *SQLE*, *DHCR24*, *HMGCS1*, *NSDHL*, and *CYP26B1* (Figure 4C and Fig. S3A) as revealed by the sequencing data. Similarly, elevations in the levels of these genes were successfully validated in the MHCC 97H and HLE cells by qPCR (Figure 4D—E). We further confirmed in the GSE25097 dataset that major genes participating in the cholesterol biosynthesis pathway presented increasing expression levels along with gradually increasing severity of liver lesions (Figure 4F). In addition to identifying the synthesis process, we also revealed the mRNA alterations in other genes involved in cholesterol homeostasis regulation in the sequencing data (Fig. S3A) and by qPCR validation (Figs. S3B—C) or online dataset confirmation (Fig. S3D), including *SREBF2* (regulation), *SOAT1* (esterification), *ABCA1* (excretion), *MYO5B* and *LIMA1* (absorption), and *APOB* and *APOC1* (trafficking). Unified expression patterns were observed by various analysis approaches. We also found that the terpenoid metabolic process, which according to KEGG (map00909) is the process upstream of steroid synthesis, was upregulated (Fig. S3E). Concerning all these findings, we preliminarily confirmed our previous assumption that cholesterol homeostasis was modified in the setting of LDLR downregulation in HCC, a modification for which the biosynthetic process was primarily responsible.

3.5. Simvastatin suppressed proliferation and metastasis of HCC cells under lower LDLR in vitro

As the initial intracellular cholesterol synthesis step, the formation of mevalonate is a rate-limiting and irreversible step in the process, which is also the target node of statins [22]. Simvastatin is considered one of the representative agents among statins [23]. Thus, we assumed that inhibition of cholesterol biosynthesis by simvastatin might decelerate the progression of HCC caused by LDLR disruption. To verify our hypothesis, we first evaluated the intracellular cholesterol level in the LDLR_KD cells by filipin staining after simvastatin treatment. In accordance with the previously mentioned results (Figure 4B), greater cholesterol accumulation was observed in the LDLR_KD groups of the MHCC 97H and HLE cells than in the corresponding control groups (Figure 5A). However, simvastatin treatment markedly reduced the elevated intracellular cholesterol content in the LDLR_KD groups (Figure 5A), which was further evidence that cholesterol biosynthesis indeed played a part in the LDL cholesterol uptake deficiency caused by LDLR downregulation (Figure 2A—C). Therefore, we further hypothesized that cholesterol synthesis disruption by simvastatin might rescue the malignant properties in the LDLR inhibition setting. Again, consistent with the aforementioned results (Figure 3A—C), augmented proliferation and migration abilities were successfully observed in the LDLR_KD groups in the MHCC 97H and HLE cells (Figure 5B—D). After simvastatin treatment, the proliferation ability, as supported by the CCK-8 and colony-formation assay results (Figure 5B—C), and the migration ability, as supported by the wound-healing assay results (Figure 5D), were apparently suppressed in the LDLR downregulation setting. Cell cycle progression and related protein levels were also inhibited by simvastatin treatment. (Figure 5E—G and Fig. S3F).

This evidence proved the valuable role of cholesterol biosynthesis in supporting augmented proliferation and metastasis of HCC cells with LDLR disruption. Moreover, simvastatin might reverse poor HCC outcomes caused by LDLR downregulation.

3.6. Activated MEK/ERK signaling pathway by lower LDLR promoted intracellular cholesterol synthesis

To mechanistically investigate how LDLR reduction affects the malignant properties of HCC cells, we performed GO enrichment analysis of the upregulated pathways. The ranking results indicated a prominent role for the MEK/ERK signaling pathway, which was the top ranked signaling cascade (Figure 6A). Protein levels of phosphorylated and total MEK1/2 and Erk1/2 were determined via Western blotting analysis. Evident activation of MEK1/2 and Erk1/2 was indicated in the LDLR_KD groups in the MHCC 97H and HLE cells (Figure 6B and Fig. S4A). We subsequently sought to determine the sequential relationship between cholesterol biosynthesis and activation of the MEK/ERK pathway. We found that additional treatment with simvastatin did not change the phosphorylation of MEK1/2 and Erk1/2 (Figure 6C and Fig. S4B). PD98059 is a well-known potent and selective inhibitor of MAP kinase kinases (MAPKK) MEK1 and MEK2 and their cascade [53]. It binds to the inactive form of MAPKK and prevents activation by upstream activators. Erk1 and Erk2 are the only known physiological substrates of MEK1/2. Thus, although it is not a direct inhibitor of Erk1/2, it is usually used to inhibit the activation of Erk1/2 [54]. We first observed an obvious inhibition efficiency on p-Erk1/2 expression by PD98059 in the LDLR_KD cells of the MHCC 97H and HLE (Fig. S4C). Then we treated the cells with PD98059 and observed the mRNA expression of representative cholesterol biosynthesis enzymes was inhibited (Figure 6D) and intracellular cholesterol levels were significantly reduced as shown by filipin staining (Figure 6E). We also evaluated the proliferation and chemotaxis phenotypes in the LDLR_KD cells and controls treated with or without PD98059. As expected, repression of activated MEK1/2 and Erk1/2 successfully reversed the malignant behaviors of MHCC 97H and HLE cells caused by downregulation of LDLR (Figure 6F—G). Collectively, these findings indicated that downregulation of LDLR promoted HCC cell proliferation and migration by activating the MEK/ERK signaling pathway, which positively regulated the cholesterol synthesis process.
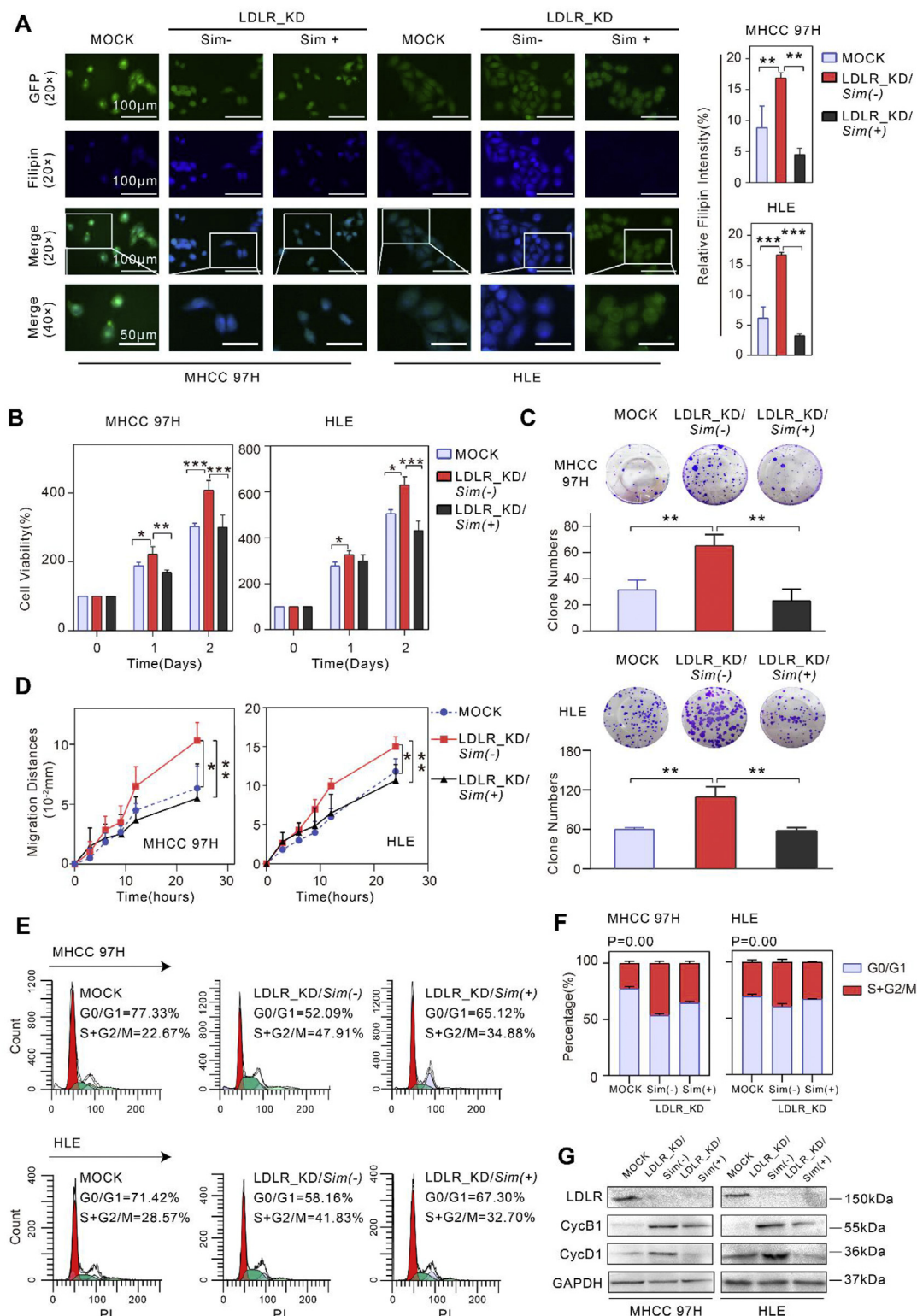
Figure 5: Blockade of cholesterol biosynthesis by simvastatin effectively suppressed proliferation and metastasis of HCC cells under lower LDLR in vitro. (A) Fluorescence micrographs and quantification bar charts of filipin staining showing the alterations of intracellular cholesterol content with or without simvastatin treatment in MHCC 97H and HLE. Scale bars, 100 μm and 50 μm. (B) Cell viability of MHCC 97H and HLE with or without simvastatin treatment detected by CCK-8 assays. (C) Representative pictures and quantification results of colony-formation assays in MHCC 97H and HLE with or without simvastatin treatment. (D) Quantification of wound-healing assays in MHCC 97H and HLE with or without simvastatin treatment. (E) The cell cycle distribution of MHCC 97H and HLE with or without simvastatin treatment. (F) The quantitative results of cell cycle distribution. (G) Western blotting of cell cycle-related proteins in MHCC 97H and HLE with or without simvastatin treatment. Data are presented as mean ± SD. *P < 0.05, **P < 0.01, and ***P < 0.001. Sim, simvastatin. All the measurements were detected in triplicate.
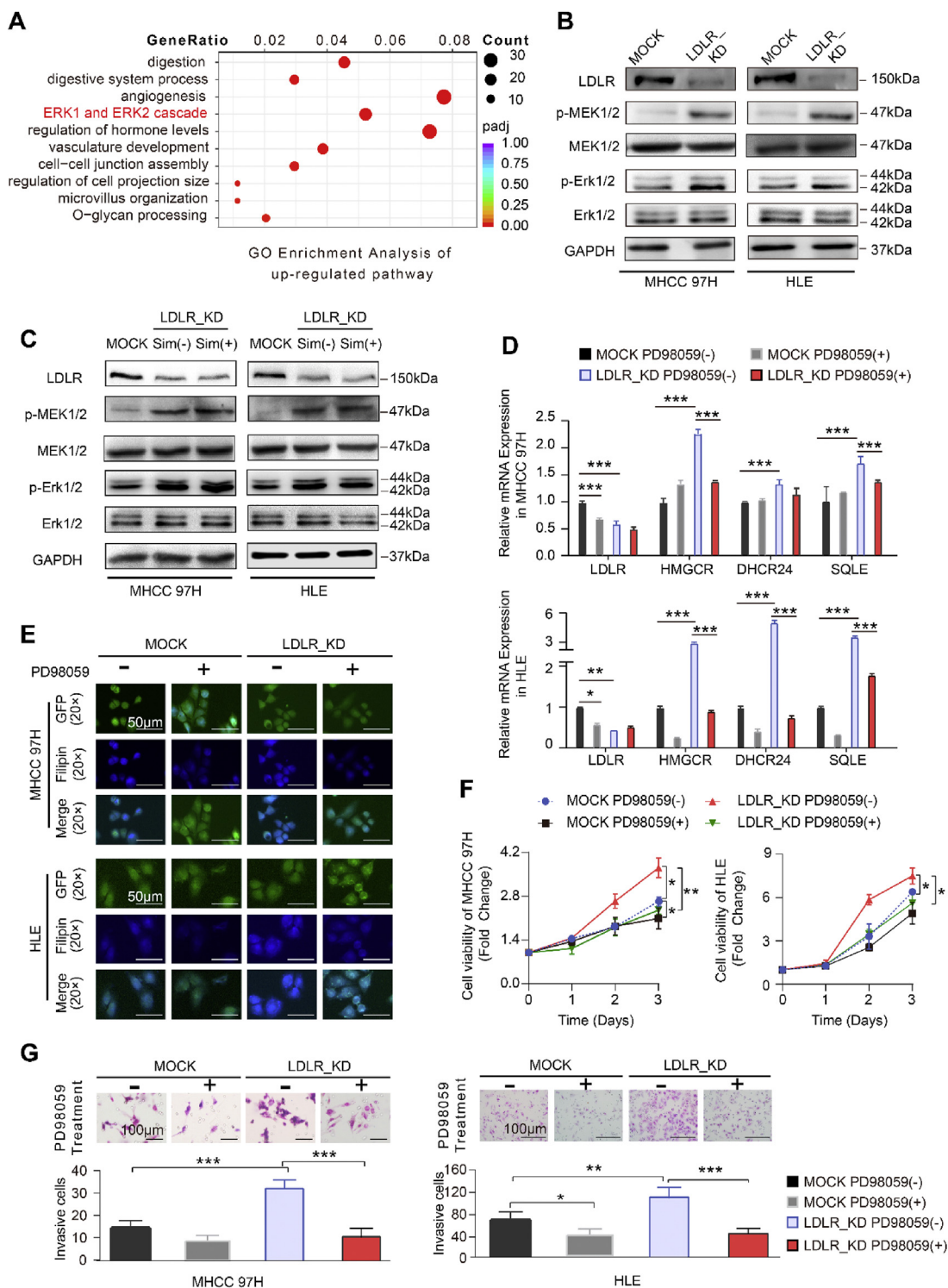
Figure 6: Activation of the MEK/ERK signaling pathway by LDLR downregulation partially contributed to intracellular cholesterol synthesis in HCC. (A) The top 10 upregulated pathways by GO enrichment analysis according to the RNA-seq results. ERK 1 and ERK 2 cascade ranked fourth. Upper x axis, gene ratio; size of point, gene count; color of point, padj of the GO terms. (B) Protein levels of phosphorylated and total MEK1/2 and Erk1/2 in MHCC 97H and HLE with differential LDLR by Western blotting. (C) Protein levels of phosphorylated and total MEK1/2 and Erk1/2 with or without simvastatin treatment in MHCC 97H and HLE. (D) RT-PCR showing mRNA expression of representative genes associated with cholesterol synthesis with or without PD98059 treatment in MHCC 97H and HLE. (E) Fluorescence micrographs of filipin staining showing the alterations of intracellular cholesterol content with or without PD98059 treatment in MHCC 97H and HLE. Scale bars, 50 μm. (F) Cell viability of MHCC 97H and HLE with or without PD98059 treatment detected by CCK-8 assays. (G) Representative pictures and quantification results of chemotaxis assays with or without PD98059 treatment in MHCC 97H and HLE. Scale bars, 100 μm and 50 μm. Data are presented as mean ± SD. *$P < 0.05$, **$P < 0.01$, and ***$P < 0.001$. Sim, simvastatin. All of the measurements were detected in triplicate. (For interpretation of the references to color in this figure legend, the reader is referred to the Web version of this article.)
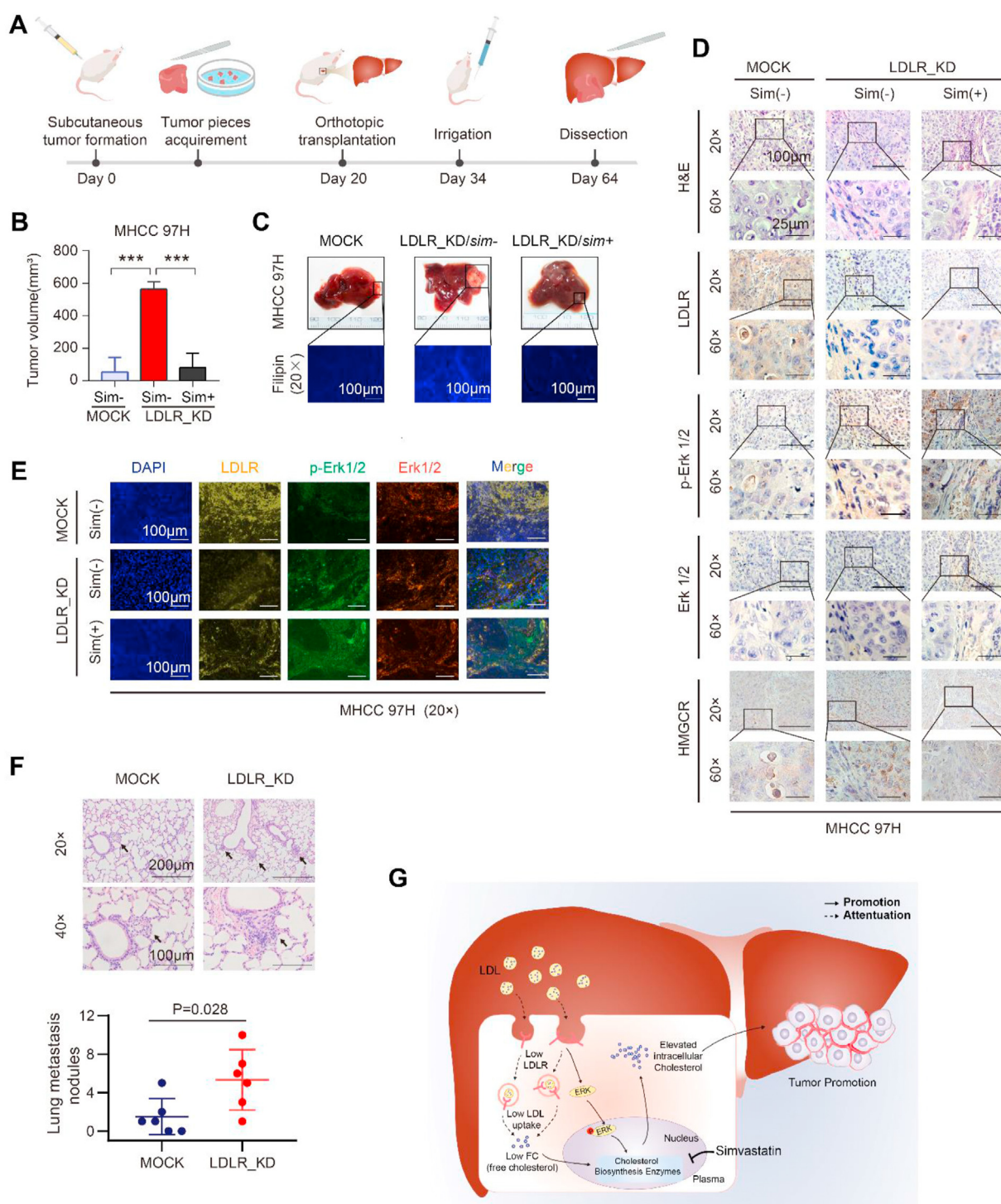
Figure 7: Downregulation of LDLR promoted HCC tumor proliferation and metastasis in vivo. (A) Flow chart of the orthotopic transplantation mouse model. (B) Quantification of tumor volume of the MOCK and LDLR_KD groups administered simvastatin or control solvent (simvastatin, 50 mg/kg/2 days). Scale bars, 100 μm. (C) Images of orthotopic tumor on the liver and matched filipin staining in the 3 groups. (D) H&E and representative IHC staining of LDLR, Erk1/2, p-Erk1/2, and HMGCR in tumor sections from the MOCK, LDLR_KD/sim-, and LDLR_KD/sim + groups. Scale bars, 100 μm and 25 μm. (E) Representative immunofluorescence pictures of LDLR, Erk1/2, and p-Erk1/2 in tumor sections from the MOCK, LDLR_KD/sim-, and LDLR_KD/sim + groups. Scale bars, 100 μm. (F) Representative H&E staining pictures of the lung metastasis nodules and quantitative scatter diagram. (G) Schematic model showing the impact of LDLR inhibition on HCC progression by activating the MEK/ERK signaling pathway and subsequently elevated intracellular cholesterol synthesis that can be targeted by simvastatin.

3.7. Downregulation of LDLR promoted HCC tumor proliferation and metastasis in vivo

We also investigated the contribution of LDLR downregulation to tumorigenesis in vivo using an orthotopic implantation model to better simulate the liver microenvironment. We first obtained tumor samples for implantation by subcutaneous injection of MHCC 97H cells with different LDLR levels. Two weeks after implantation of tumor slices onto the liver surface, we started treatment with simvastatin or control solvent every two days. Four weeks later after administration, we sacrificed all of the mice and evaluated tumor formation (Figure 7A). According to the in vitro results, the tumor size was notably increased in the LDLR_KD groups compared to the MOCK group but was appreciably reduced by simvastatin administration (Figure 7B). Filipin staining of the paraffin sections also indicated the obvious accumulation of cholesterol, which was effectively ameliorated by simvastatin (Figure 7C). At the tissue level, we characterized identical stronger staining of p-Erk1/2 in the LDLR_KD groups compared to the MOCK group regardless of simvastatin treatment (Figure 7D—E). HMGCR staining was also enhanced in the LDLR_KD groups, which could be inhibited with simvastatin (Figure 7D). According to the lung metastasis mouse model, downregulation of LDLR efficiently promoted the metastasis ability of MHCC 97H, which exhibited more lung metastatic nodules by H&E staining (Figure 7F). Collectively, these results indicated that LDLR reduction facilitated HCC progression by activating the MEK/ERK signaling pathway and sequential cholesterol biosynthesis elevation in vivo. Blockade of cholesterol synthesis by simvastatin effectively attenuated HCC progression in vivo.

3.8. Angiogenesis was involved in advancing HCC with the MEK/ERK pathway in a converging manner

The GO enrichment analysis also revealed an important role of angiogenesis in LDLR_KD cells (Figure 4A and Figure 6A). We then investigated whether the LDLR expression would influence the angiogenesis in HCC. The expression pattern of LDLR and CD31 in the Ye liver cohort from the Oncomine database revealed a relatively lower LDLR level and a higher CD31 level in HCC patients with portal vein metastases compared with intrahepatic metastasis or no metastasis cases (Supplementary Figs. 5A—B). We also tested the pro-angiogenesis ability in MHCC 97H with different LDLR levels. We validated the tubule formation ability and proliferation of HUVEC cultured by MHCC 97H conditional medium under different LDLR levels. Stronger angiogenesis and proliferation abilities were observed in the LDLR_KD conditional medium (Figs. S5C—D). Tubule formation did not change much after culturing under LDLR_KD conditional medium treated with PD98059 (Fig. S5E), which partially indicated that the angiogenesis and MEK/ERK pathways might present parallel in HCC with lower LDLR expression. They were involved in advancing HCC in a converging manner. The related mechanisms and relationship between the different pathways caused by LDLR downregulation need further exploration.

Considering all the previously mentioned findings, we conclusively demonstrated that LDLR inhibition effectively promoted HCC proliferation and metastasis by enhancing the intracellular cholesterol biosynthesis process in a manner partially attributed to the activation of the MEK/ERK signaling pathway. Inhibition of cholesterol synthesis with simvastatin efficiently curbed malignant behaviors in the setting of lower LDLR expression (Figure 7G).

4. DISCUSSION

Cancer is intrinsically a disturbance of cell proliferation and migration. During continuous uncontrolled biological activities, adaptive remodeling of energy metabolism is urgently required [7]. Existing studies recognize the critical role of lipid resources in cancer progression [24]. A thorough description of how cancer cells exploit their lipid resources might provide new metabolic strategies to reinforce current anti-tumor approaches. As one of the most common lipids supporting cell growth and proliferation, cholesterol possesses multiple physiological functions in biological activities [15]. Thus, more attention is devoted to its role in cancer progression than the roles of other lipids [25—27].

LDLR was the first identified member of the low-density lipoprotein receptor (LDLR) family, which consists of several single transmembrane glycoproteins [17]. Characterized as a cluster of cell surface endocytic receptors, these proteins are mainly responsible for the internalization of lipoproteins, exotoxins, and other extracellular ligands for degradation by lysosomes [28]. LDLR is mainly responsible for the endocytosis of cholesterol-rich LDL, 70% of which occurs in the liver [29]. Normally, LDLR is located in clathrin-coated pits. Rapid recycling of LDLR from the cell surface to the intracellular space makes serum cholesterol available to cells [30]. Physiological functions endow LDLR with unavoidable effects on intracellular and serum cholesterol metabolism. Surveys have demonstrated the associations of LDLR with many cancers. For instance, lower LDLR expression has been described to indicate worse clinical outcomes in prostate and cervical cancer [18,19]. In HCC, a lower expression of LRP1, another LDLR family member, was also found to be associated with poorer prognosis, which was independently related to a shorter overall survival time and a higher tumor recurrence rate. An in vitro study also suggested an inverse correlation of LRP1 expression with cell metastatic potential in HCC [31]. Ldlr $-/-$ mice fed a Western diet were commonly used as a model to induce non-alcoholic steatohepatitis (NASH), which may cause hepatic steatosis, fibrosis, and tumorigenesis [55]. Familial hyperlipidemia (FH) commonly caused by LDLR gene mutation may underlie fatty liver disease, one of the risk factors of HCC [56]. Ethanol consumption combined with HBV persistence together synergistically enhanced cholesterol biosynthesis and decrease cholesterol utilization and uptake by downregulating LDLR and increasing CYP-7α [57]. In this study, we conducted a systematic analysis of the LDLR expression profile in HCC and characterized decreased expression in cancer tissues compared to the non-cancerous region in the databases and clinical samples. LDLR is an independent risk factor for DFS and OS in HCC. Thus, we preliminarily concluded that downregulation of LDLR might be a negative prognostic factor in human HCC.

The processes through which mammalian cells acquire cholesterol mainly consist of exogenous lipoprotein intake and endogenous de novo synthesis from acetyl-coenzyme A [7]. However, how cancer cells manipulate these programs is still unclear. Based on TCGA analysis, enhanced activity of the cholesterol synthesis pathway was discovered to be correlated with poor patient survival in sarcoma, melanoma, and acute myeloid leukemia, but the opposite correlation was observed in lower grade glioma [3]. In ALK + ALCLs with cholesterol synthesis deficiency caused by loss of squalene monooxygenase, cholesterol uptake mediated by LDLR was identified as the essential mode of cancer cell growth [11]. In HCC, elevation of SQLE, which is one of the rate-limiting enzymes in the cholesterol synthesis pathway, has been identified to be associated with poor patient outcomes [32]. A high expression of DHCR24 was also identified in human HCC, which correlated with poor clinical outcomes. Downregulation of DHCR24 inhibited growth and migration of HCC cells [58]. Cholesterol biosynthesis was also found to play a major role in the growth of HCCs with fatty acid synthase depletion [33]. Thus, the precise roles of different

cholesterol acquisition modes in tumor progression appear to be cancer-type specific. Other cholesterol metabolic pathways are also reshaped in HCC for cells to obtain more cholesterol. For example, ABCA8, which works as a transmembrane transporter mediating cholesterol efflux, was downregulated in HCC. Overexpression of ABCA8 inhibited HCC progression and thus may work as a negative prognostic factor of HCC [59]. Jianwen Jiang et al. established four HCC subtypes: cholesterogenic, glycolytic, mixed, and quiescent based on a TCGA analysis. The prognosis of the cholesterogenic subgroup was poorer [60]. In this study, we found that intracellular cholesterol evidently accumulated under LDL uptake dysregulation caused by lower LDLR in the HCC cell lines. Mechanistically, we demonstrated that cholesterol biosynthesis was the chief contributor to the intracellular cholesterol elevation and induction of malignant behaviors in the HCC cell lines when lower exogenous cholesterol was available. We also identified several other cholesterol metabolic changes, for example cholesterol esterification, excretion, absorption, and trafficking. These remodeling methods provided adequate cholesterol for HCC cells to utilize. Therefore, we supplemented the cognition on understanding cholesterol metabolism rewiring in HCC.

Originally approved to treat cardiovascular disease, statins are canonical inhibitors of cholesterol synthesis. Numerous preclinical or epidemiological studies have generally suggested cancer-preventive or therapeutic effects of statins in a series of cancer types, such as colorectal cancer [34], lung cancer [35], and melanoma [36]. Statin use was found to be negatively correlated with the risk of HCC independent of different pathogenies [37—39]. As one of the representative statins, simvastatin also has a positive therapeutical effect on many types of cancers by inhibiting cell growth and motility or decreasing resistance to chemotherapeutic drugs [40,41]. In our study, we revealed that cholesterol biosynthetic activity increased when LDLR was downregulated and was the major contributor to intracellular cholesterol accumulation. Simvastatin effectively decreased the level of cholesterol and significantly inhibited the proliferation and migration of HCC cells with lower LDLR levels in vitro, consistent with previous reports [42,43]. We also discovered in vivo that simvastatin efficiently inhibited orthotopic tumor proliferation caused by LDLR downregulation, which indicated clinical promise for simvastatin in HCC patients with lower LDLR expression. Thus, these findings suggest a preliminary strategy for treating HCC patients with additional clinical use of lipid-lowering agents, which may offer a metabolism-based therapeutic landscape.

Canonical intracellular cholesterol regulation strongly depends on the intracellular cholesterol level, although the homeostatic mechanisms involved are only partially illuminated. After sensing a low intracellular cholesterol level in the endoplasmic reticulum, cleaved SREBP migrates to the nucleus and sequentially initiates the transcription of target genes by binding to sterol regulatory elements (SREs), a process that can be terminated under high cholesterol levels [44]. Cholesterol biosynthesis has been claimed to have intricate connections with oncogenic factors and tumor suppressors [6]. Multiple oncogenic signaling pathways, such as the TP53, PI3K-AKT, and RAS-MAPK pathways, have been indicated to affect cholesterol biosynthesis in various types of cancer, including HCC [3,45—49]. Existing studies have also recognized the critical role of the MAP kinase Erk1/2 in promoting cholesterol biosynthesis in HCC, either by activating HSF1 [42] or phosphorylating SREBP2 at serine 432 and serine 455 [50]. In this study, we found that the MEK/ERK signaling pathway was upregulated in the setting of LDLR downregulation by transcriptome sequencing. Inhibition of phosphorylated Erk1/2 activity by PD98059 efficiently reduced the mRNA

levels of representative cholesterol biosynthesis genes and in turn the intracellular cholesterol concentration. Simvastatin treatment did not affect the phosphorylation of Erk1/2 in vitro and in vivo, which suggested that the MEK/ERK signaling pathway partially contributed to increasing cholesterol synthesis. The precise link between LDLR expression and stimulation of the MEK/ERK pathway merits further investigation.

The cholesterol level tends to be increased in cancer cells [25]. Interestingly, serum cholesterol may also exert a considerable influence on cancer progression. Recent evidence suggested an obvious reinforcement of the anti-tumor ability of NK cells in HCC caused by high serum cholesterol [51]. Other researchers posit that intracellular cholesterol may account for more cancer burden than cholesterol in the circulation [45,52]. In this study, we found a slight elevation of LDL-C in the culture medium after decreasing the LDLR expression in the HCC cell lines. However, we did not detect a direct link between LDLR levels and serum cholesterol (data not shown), which partially confirmed that downregulation of LDLR might contribute to HCC progression mostly by affecting intracellular cholesterol homeostasis rather than serum cholesterol levels.

5. CONCLUSION

In summary, we primarily conducted a systematic analysis of the LDLR expression profile in HCC and identified LDLR downregulation as a negative prognostic factor in HCC. Downregulation of LDLR may elevate intracellular cholesterol synthesis to accelerate proliferation and motility via a mechanism partially attributed to stimulation of the MEK/ERK signaling pathway. Additionally, by suppressing the cholesterol synthesis process, simvastatin efficiently decreased the intracellular cholesterol level and in turn blocked the malignant phenotypes of HCC cells. Thus, repression of intracellular cholesterol synthesis with statins might be a promising therapeutic approach for HCC with lower LDLR. Alternatively, disruption of both cholesterol uptake and the intracellular synthesis process may provide metabolic insight for guiding the clinical treatment of HCC.

AVAILABILITY OF DATA AND MATERIALS

The datasets used and analyzed during this study are available from the corresponding authors on reasonable request.

FUNDING

ROLE OF FUNDING SOURCES

Dr. Hua Guo contributed to the study concept, design, and manuscript revisions.

CONFLICT OF INTEREST

None declared.

APPENDIX A. SUPPLEMENTARY DATA

Supplementary data to this article can be found online at https://doi.org/10.1016/j.molmet.2021.101230.

Original Article

REFERENCES

[1] Hanahan, D., Weinberg, R.A., 2000. The hallmarks of cancer. Cell 100:57—70.

[2] Hanahan, D., Weinberg, R.A., 2011. Hallmarks of cancer: the next generation. Cell 144:646—674.

[3] Kuzu, O.F., Noory, M.A., Robertson, G.P., 2016. The role of cholesterol in cancer. Cancer Research 76:2063—2070.

[4] Warburg, O., 1956. On the origin of cancer cells. Science 123:309—314.

[5] Mankoff, D.A., Eary, J.F., Link, J.M., Muzi, M., Rajendran, J.G., Spence, A.M., et al., 2007. Tumor-specific positron emission tomography imaging in patients: [18F] fluorodeoxyglucose and beyond. Clinical Cancer Research 13:3460—3469.

[6] Kroemer, G., Pouyssegur, J., 2008. Tumor cell metabolism: cancer's Achilles' heel. Cancer Cell 13:472—482.

[7] Riscal, R., Skuli, N., Simon, M.C., 2019. Even cancer cells watch their cholesterol! Molecular Cell 76:220—231.

[8] Wang, H.Q., Altomare, D.A., Skele, K.L., Poulikakos, P.I., Kuhajda, F.P., Di Cristofano, A., et al., 2005. Positive feedback regulation between AKT activation and fatty acid synthase expression in ovarian carcinoma cells. Oncogene 24:3574—3582.

[9] Luo, J., Yang, H., Song, B.L., 2020. Mechanisms and regulation of cholesterol homeostasis. Nature Reviews Molecular Cell Biology 21:225—245.

[10] Ma, L., Wang, L., Nelson, A.T., Han, C., He, S., Henn, M.A., et al., 2020. 27-Hydroxycholesterol acts on myeloid immune cells to induce T cell dysfunction, promoting breast cancer progression. Cancer Letters 493:266—283.

[11] Garcia-Bermudez, J., Baudrier, L., Bayraktar, E.C., Shen, Y., La, K., Guarecuco, R., et al., 2019. Squalene accumulation in cholesterol auxotrophic lymphomas prevents oxidative cell death. Nature 567:118—122.

[12] Guillaumond, F., Bidaut, G., Ouaissi, M., Servais, S., Gouirand, V., Olivares, O., et al., 2015. Cholesterol uptake disruption, in association with chemotherapy, is a promising combined metabolic therapy for pancreatic adenocarcinoma. Proceedings of the National Academy of Sciences of the U S A 112:2473—2478.

[13] Liang, J.Q., Teoh, N., Xu, L., Pok, S., Li, X., Chu, E.S.H., et al., 2018. Dietary cholesterol promotes steatohepatitis related hepatocellular carcinoma through dysregulated metabolism and calcium signaling. Nature Communications 9:4490.

[14] Jiang, Y., Sun, A., Zhao, Y., Ying, W., Sun, H., Yang, X., et al., 2019. Chinese Human Proteome Project, Proteomics identifies new therapeutic targets of early-stage hepatocellular carcinoma. Nature 567:257—261.

[15] Razin, S., Tully, J.G., 1970. Cholesterol requirement of mycoplasmas. Journal of Bacteriology 102:306—310.

[16] Catapano, A.L., 1989. The low density lipoprotein receptor: structure, function and pharmacological modulation. Pharmacology & Therapeutics 43:187—219.

[17] Jeon, H., Blacklow, S.C., 2005. Structure and physiologic function of the low-density lipoprotein receptor. Annual Review of Biochemistry 74:535—562.

[18] Stopsack, K.H., Gerke, T.A., Andren, O., Andersson, S.O., Giovannucci, E.L., Mucci, L.A., et al., 2017. Cholesterol uptake and regulation in high-grade and lethal prostate cancers. Carcinogenesis 38:806—811.

[19] Sun, Y., Feng, Y., Zhang, G., Xu, Y., 2019. The endonuclease APE1 processes miR-92b formation, thereby regulating expression of the tumor suppressor LDLR in cervical cancer cells. Ther Adv Med Oncol 11, 1758835919855859.

[20] Chen, L., Guo, P., He, Y., Chen, Z., Chen, L., Luo, Y., et al., 2018. HCC-derived exosomes elicit HCC progression and recurrence by epithelial-mesenchymal transition through MAPK/ERK signaling pathway. Cell Death & Disease 9:513.

[21] Caballero, F., Fernandez, A., De Lacy, A.M., Fernandez-Checa, J.C., Caballeria, J., Garcia-Ruiz, C., 2009. Enhanced free cholesterol, SREBP-2 and StAR expression in human NASH. Journal of Hepatology 50:789—796.

[22] Gobel, A., Rauner, M., Hofbauer, L.C., Rachner, T.D., 2020. Cholesterol and beyond - the role of the mevalonate pathway in cancer biology. Biochimica et Biophysica Acta (BBA) - Reviews on Cancer 1873:188351.

[23] Slater, E.E., MacDonald, J.S., 1988. Mechanism of action and biological profile of HMG CoA reductase inhibitors. A New Therapeutic Alternative Drugs 36(Suppl 3):72—82.

[24] Li, H., Feng, Z., He, M.L., 2020. Lipid metabolism alteration contributes to and maintains the properties of cancer stem cells. Theranostics 10:7053—7069.

[25] Jun, S.Y., Brown, A.J., Chua, N.K., Yoon, J.Y., Lee, J.J., Yang, J.O., et al., 2020. Reduction of squalene epoxidase by cholesterol accumulation accelerates colorectal cancer progression and metastasis. Gastroenterology.

[26] Hong, C.S., Jeong, E., Boyiadzis, M., Whiteside, T.L., 2020. Increased small extracellular vesicle secretion after chemotherapy via upregulation of cholesterol metabolism in acute myeloid leukaemia. Journal of Extracellular Vesicles 9:1800979.

[27] Kim, J., Dey, A., Malhotra, A., Liu, J., Ahn, S.I., Sei, Y.J., et al., 2020. Engineered biomimetic nanoparticle for dual targeting of the cancer stem-like cell population in sonic hedgehog medulloblastoma. Proceedings of the National Academy of Sciences of the U S A 117:24205—24212.

[28] Willnow, T.E., Nykjaer, A., Herz, J., 1999. Lipoprotein receptors: new roles for ancient proteins. Nature Cell Biology 1:E157—E162.

[29] Goldstein, J.L., Brown, M.S., 2009. The LDL receptor. Arteriosclerosis, Thrombosis, and Vascular Biology 29:431—438.

[30] Basu, S.K., Goldstein, J.L., Anderson, R.G., Brown, M.S., 1981. Monensin interrupts the recycling of low density lipoprotein receptors in human fibroblasts. Cell 24:493—502.

[31] Huang, X.Y., Shi, G.M., Devbhandari, R.P., Ke, A.W., Wang, Y., Wang, X.Y., et al., 2012. Low level of low-density lipoprotein receptor-related protein 1 predicts an unfavorable prognosis of hepatocellular carcinoma after curative resection. PloS One 7:e32775.

[32] Liu, D., Wong, C.C., Fu, L., Chen, H., Zhao, L., Li, C., et al., 2018. Squalene epoxidase drives NAFLD-induced hepatocellular carcinoma and is a pharmaceutical target. Science Translational Medicine 10.

[33] Che, L., Chi, W., Qiao, Y., Zhang, J., Song, X., Liu, Y., et al., 2020. Cholesterol biosynthesis supports the growth of hepatocarcinoma lesions depleted of fatty acid synthase in mice and humans. Gut 69:177—186.

[34] Poynter, J.N., Gruber, S.B., Higgins, P.D., Almog, R., Bonner, J.D., Rennert, H.S., et al., 2005. Statins and the risk of colorectal cancer. New England Journal of Medicine 352:2184—2192.

[35] Abstracts of the 30th annual meeting of the American society of primatologists. June 20-23, 2007. Winston-salem, North Carolina, USA. American Journal of Primatology 69(Suppl 1), 2007:30—132.

[36] Demierre, M.F., Higgins, P.D., Gruber, S.B., Hawk, E., Lippman, S.M., 2005. Statins and cancer prevention. Nature Reviews Cancer 5:930—942.

[37] Singh, S., Singh, P.P., Singh, A.G., Murad, M.H., Sanchez, W., 2013. Statins are associated with a reduced risk of hepatocellular cancer: a systematic review and meta-analysis. Gastroenterology 144:323—332.

[38] Tsan, Y.T., Lee, C.H., Ho, W.C., Lin, M.H., Wang, J.D., Chen, P.C., 2013. Statins and the risk of hepatocellular carcinoma in patients with hepatitis C virus infection. Journal of Clinical Oncology 31:1514—1521.

[39] Tsan, Y.T., Lee, C.H., Wang, J.D., Chen, P.C., 2012. Statins and the risk of hepatocellular carcinoma in patients with hepatitis B virus infection. Journal of Clinical Oncology 30:623—630.

[40] Wang, S.T., Ho, H.J., Lin, J.T., Shieh, J.J., Wu, C.Y., 2017. Simvastatin-induced cell cycle arrest through inhibition of STAT3/SKP2 axis and activation of AMPK to promote p27 and p21 accumulation in hepatocellular carcinoma cells. Cell Death & Disease 8:e2626.

[41] Paajarvi, G., Roudier, E., Crisby, M., Hogberg, J., Stenius, U., 2005. HMG-CoA reductase inhibitors, statins, induce phosphorylation of Mdm2 and attenuate the p53 response to DNA damage. The FASEB Journal 19:476—478.

[42] Kang, H., Oh, T., Bahk, Y.Y., Kim, G.H., Kan, S.Y., Shin, D.H., et al., 2019. HSF1 regulates mevalonate and cholesterol biosynthesis pathways. Cancers, 11.

[43] Kim, Y.S., Lee, Y.M., Oh, T.I., Shin, D.H., Kim, G.H., Kan, S.Y., et al., 2018. Emodin sensitizes hepatocellular carcinoma cells to the anti-cancer effect of sorafenib through suppression of cholesterol metabolism. International Journal of Molecular Sciences 19.

[44] Espenshade, P.J., Hughes, A.L., 2007. Regulation of sterol synthesis in eu-karyotes. Annual Review of Genetics 41:401–427.

[45] Freed-Pastor, W.A., Mizuno, H., Zhao, X., Langerod, A., Moon, S.H., Rodriguez-Barrueco, R., et al., 2012. Mutant p53 disrupts mammary tissue architecture via the mevalonate pathway. Cell 148:244–258.

[46] Parrales, A., Thoenen, E., Iwakuma, T., 2018. The interplay between mutant p53 and the mevalonate pathway. Cell Death & Differentiation 25:460–470.

[47] Moon, S.H., Huang, C.H., Houlihan, S.L., Regunath, K., Freed-Pastor, W.A., Morris, J.P.t., et al., 2019. p53 represses the mevalonate pathway to mediate tumor suppression. Cell 176:564–580 e519.

[48] Yue, S., Li, J., Lee, S.Y., Lee, H.J., Shao, T., Song, B., et al., 2014. Cholesteryl ester accumulation induced by PTEN loss and PI3K/AKT activation underlies human prostate cancer aggressiveness. Cell Metabolism 19:393–406.

[49] Chan, L.K., Wai-Hung Ho, D., Kam, C.S., Yung-Tuen Chiu, E., Lai-Oi Lo, I., Tsz-Wai Yau, D., et al., 2020. RSK2-inactivating mutations potentiate MAPK signaling and support cholesterol metabolism in hepatocellular carcinoma. Journal of Hepatology.

[50] Kotzka, J., Lehr, S., Roth, G., Avci, H., Knebel, B., Muller-Wieland, D., 2004. Insulin-activated Erk-mitogen-activated protein kinases phosphorylate sterol regulatory element-binding Protein-2 at serine residues 432 and 455 in vivo. Journal of Biological Chemistry 279:22404–22411.

[51] Qin, W.H., Yang, Z.S., Li, M., Chen, Y., Zhao, X.F., Qin, Y.Y., et al., 2020. High serum levels of cholesterol increase antitumor functions of nature killer cells and reduce growth of liver tumors in mice. Gastroenterology 158:1713–1727.

[52] Sorrentino, G., Ruggeri, N., Specchia, V., Cordenonsi, M., Mano, M., Dupont, S., et al., 2014. Metabolic control of YAP and TAZ by the mevalonate pathway. Nature Cell Biology 16:357–366.

[53] Zhong, S., Li, L., Liang, N., Zhang, L., Xu, X., Chen, S., et al., 2021. Acetal-dehyde Dehydrogenase 2 regulates HMG-CoA reductase stability and cholesterol synthesis in the liver. Redox Biol 41:101919.

[54] Lu, C.W., Yabuuchi, A., Chen, L., Viswanathan, S., Kim, K., Daley, G.Q., 2008. Ras-MAPK signaling promotes trophectoderm formation from embryonic stem cells and mouse embryos. Nature Genetics 40:921–926.

[55] Garcia-Jaramillo, M., Lytle, K.A., Spooner, M.H., Jump, D.B., 2019. A lipidomic analysis of docosahexaenoic acid (22:6, omega3) mediated attenuation of western diet induced nonalcoholic steatohepatitis in male ldlr (-/-) mice. Metabolites 9.

[56] Liebe, R., Esposito, I., Bock, H.H., Dahl, S.V., Stindt, J., Baumann, U., et al., 2021. Diagnosis and management of secondary causes of steatohepatitis. Journal of Hepatology.

[57] Wang, Y., Wu, T., Hu, D., Weng, X., Wang, X., Chen, P.J., et al., 2018. Intracellular hepatitis B virus increases hepatic cholesterol deposition in alcoholic fatty liver via hepatitis B core protein. The Journal of Lipid Research 59:58–68.

[58] Wu, J., Guo, L., Qiu, X., Ren, Y., Li, F., Cui, W., et al., 2020. Genkwadaphnin inhibits growth and invasion in hepatocellular carcinoma by blocking DHCR24-mediated cholesterol biosynthesis and lipid rafts formation. British Journal of Cancer 123:1673–1685.

[59] Cui, Y., Liang, S., Zhang, S., Zhang, C., Zhao, Y., Wu, D., et al., 2020. ABCA8 is regulated by miR-374b-5p and inhibits proliferation and metastasis of hepa-tocellular carcinoma through the ERK/ZEB1 pathway. Journal of Experimental & Clinical Cancer Research 39:90.

[60] Jiang, J., Zheng, Q., Zhu, W., Chen, X., Lu, H., Chen, D., et al., 2020. Al-terations in glycolytic/cholesterogenic gene expression in hepatocellular car-cinoma. Aging 12:10300–10316.